Phononic Weyl nodal straight lines in MgB_2

Jiangxu Li,[1,2] Qing Xie,[1,3] Jiaxi Liu,[1,2] Ronghan Li,[1] Min Liu,[1,2] Lei Wang,[1,2]
Dianzhong Li,[1] Yiyi Li,[1] and Xing-Qiu Chen[1,*]
[1]*Shenyang National Laboratory for Materials Science, Institute of Metal Research, Chinese Academy of Sciences, Shenyang 110016, China*
[2]*School of Materials Science and Engineering, University of Science and Technology of China, Shenyang 110016, China*
[3]*University of Chinese Academy of Sciences, Beijing 100049, China*

(Received 18 January 2018; published 3 January 2020; corrected 25 June 2020)

Based on first-principles calculations, we predict that the superconductor MgB_2 with an AlB_2-type centrosymmetric lattice hosts the so-called phononic topological Weyl nodal lines (PTWNLs) in its bulk phonon spectrum. These PTWNLs can be viewed as countless Weyl points (WPs) closely aligned along the straight lines in the $-H$-K-H direction within the three-dimensional Brillouin zone (BZ) and are always paired with opposite Berry phase. Their topologically nontrivial natures are confirmed by the calculated Berry curvature distributions on the planes perpendicular to these lines. These lines are unique, because they are located exactly at the high-symmetry boundary of the BZ protected by the mirror symmetry and, simultaneously, are straightly transverse to the whole BZ, differently from known classifications, including nodal rings, nodal chains or nets, and nodal loops. On the $(10\bar{1}0)$ crystal surface, the PTWNL-induced drumhead-like nontrivial surface states appear within the rectangular area confined by the projected lines of the PTWNLs. Moreover, when the mirror symmetry is broken, the double-degenerate PTWNLs are further lifted to form a pair of WPs with opposite chirality. Our results pave the way for future experimental study of topological phonons on MgB_2 and highlight similar results in a series of isostructural AlB_2-type metallic diborides.

DOI: 10.1103/PhysRevB.101.024301

I. INTRODUCTION

Accompanying extensive studies of topological insulators, topological semimetals, and even topological superconductors in their electronic structures [1–3], topological phonons [4–9] have most recently attracted attention in condensed matter physics and material sciences. This is mainly because topological phononic states will be interesting for potential applications. Differently from various electronic fermions, phonons, being among the bosons, are not limited by the Pauli exclusion principle. This means that the whole frequency zone of a phonon spectrum can be physically probed. Similarly to topological properties of electrons, the topological effects of phonons can induce one-way edge phonon states or topologically protected surface phononic states. Physically, these states will conduct phonon with little or no scattering [4,5], suggesting possible applications for designing phononic circuits [6]. For instance, utilizing the one-way edge phonon states, an ideal phonon diode [6] was proposed with a fully 100% efficiency in a multiterminal transport system. Due to the forward- or backward-moving states, the heat transportation will have directivity and one-way states, which can hold the perfect diode effect between two terminals. This offers an ideal example for experiments to detect the topological straight nodal line, which is stabilized by crystal symmetry. It can also be extended to the field of photonics and acoustics. Due to the stability of the topological nodal line, it can be immune to any symmetry-preserving perturbation and can be possibly used to control heat, photons, and sound. It was even theoretically uncovered that the chirality of topological phonons excited by polarized photons can be detected by a valley phonon Hall effect in monolayer hexagonal lattices [9]. In particular, it needs to be emphasized that, similarly to various fermions of electrons, exciting progress with respect to bosons (vibrational phonons) has been also predicted [7] or observed in the three-dimensional (3D) momentum space of solid crystals with topological vibrational states, such as Dirac, Weyl, and line-node phonons in photonic crystals with macroscopic acoustic systems of kHz frequency [4,5,7,10–22] and theoretically predicted doubly-Weyl phonons in transition-metal monosilicides with atomic vibrations at THz frequency [23]. Most recently, also in a series of WC-type materials (i.e., TiS, ZrSe and HfTe) with atomic vibration at THz frequency, single topological Weyl phonons were predicted, and they exist opening topological arcs of surface phonons, connecting pairs of surface-projected Weyl points (WPs) with opposite chirality [24,25]. However, to date no phononic topological Weyl nodal lines have been reported in macroscopic acoustic systems at kHz frequency or in atomic vibrational periodic lattices at THz frequency.

It needs to be emphasized that topological nodal lines [26] have been already extensively studied in electronic band structures, optical lattices, and photonic and acoustic systems. To date, nodal lines have been classified into various categories, such as (*i*) isolated closed nodal rings in alkaline earth metals of hcp Be and Mg [27,28] and of fcc Ca and Sr [28,29], in the TiSi family [30], in 3D carbon allotropes [31], in antiperovskite Cu_3(Pb, Zn)N [32,33], in Ca_3P_2 [34], in photonic crystals [7], and in a hyperhoneycomb lattice [35];

*xingqiu.chen@imr.ac.cn

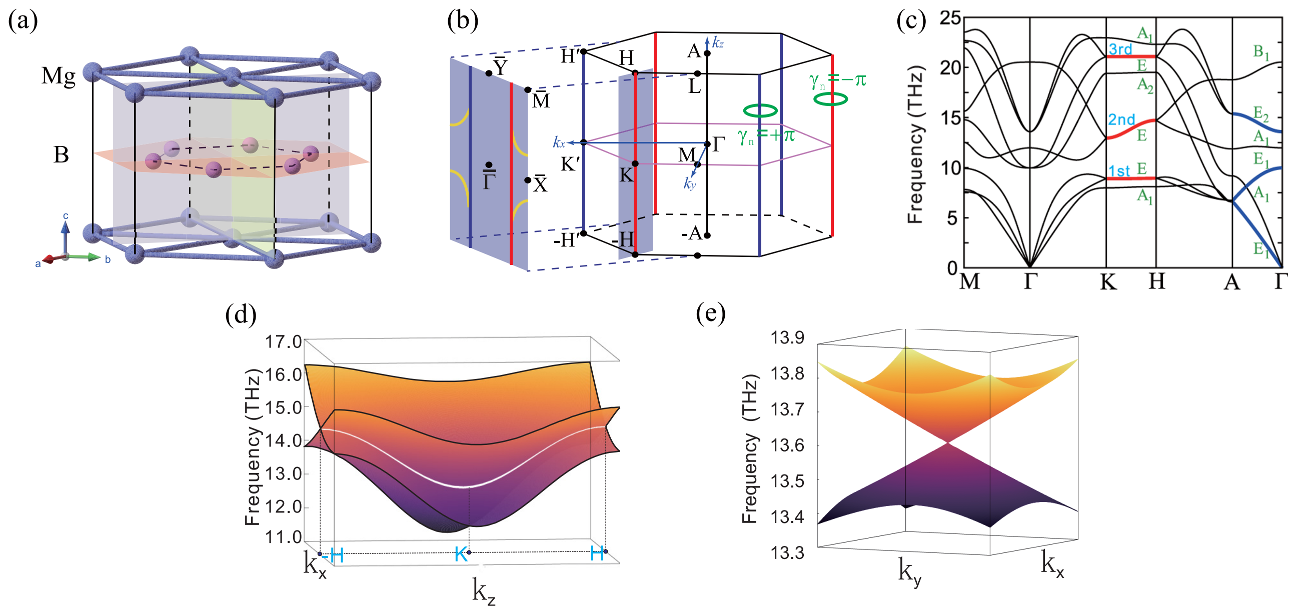

FIG. 1. (a) Crystal structure of MgB_2. Three shadowed planes are the mirror planes. (b) The Brillouin zone and $(10\bar{1}0)$ surface. The PTWNLs traverse the whole BZ along both the $-H$ to H and the $-H'$ to H' directions. Red (blue) lines have negative (positive) Berry phase. Each PTWNL extends through the whole BZ one time along one of the directions with opposite Berry phase. The surface states at about 14.2 THz are schematically depicted on the surface. (c) The phonon dispersion of MgB_2 along the high-symmetry momentums paths in the BZ. Three red thick bands (marked as 1st, 2nd, and 3rd) along the H-K direction correspond to double-degenerate PTWNLs, whereas three blue thick double-generate bands along the Γ-A direction are topologically trivial. (d) Three-dimensional phononic bands around the second PTWNL on the shaded k plane across the $-H$-K-H direction as shown in the 3D BZ in panel (b). (e) Three-dimensional phononic bands at any WP on any PTWNL. Here, we visualize them by selecting a node on the second PTWNL at $k_z = 0.2$.

(*ii*) nodal chains or nodal nets in which several closed nodal rings touch at a point to form a chain (or a net) stretching in the whole BZ of iridium tetrafluoride [36], HfC [37], graphene network structure [38], TiS [24], TiB_2, and ZrB_2 [39–41]; (*iii*) nodal links [42] featuring closed nodal loops which are linked and interwound with each other in a so-called nodal-link semimetal [42] or the Hopf-link semimetal Co_2MnGa [43]; and (*iv*) nodal knots in which a single nodal ring entangles with itself [44]. Besides these four main types of nodal lines structures, some discontinuous nodal lines can also exists in the BZ, such as in monoclinic C_{16} [45] and metallic rutile oxides [46]. To date, no Weyl nodal *straight* lines have been reported.

Within this context, through first-principles calculations [47], we report that the famous high-temperature BCS-type superconductor MgB_2 [48,49], hosts phononic topological Weyl nodal straight lines (PTWNLs) in its bulk BZ of the phonon spectrum. These PTWNLs are always paired with opposite Berry phase along the high-symmetry $-H$-K-H and $-H'$-K'-H' boundaries of the 3D BZ, extending the whole BZ through the one-way direction [Fig. 1(b)]. The Berry phases of these PTWNLs are $\pm\pi$, indicating their nontrivial topological nature. On the $(10\bar{1}0)$ surface, we observe PTWNL-induced drumhead-like nontrivial surface states confined in rectangular-shape regions formed by the projected lines of the bulk PTWNLs. When the inversion symmetry is broken, the double-degenerate PTWNLs would be further lifted up and WPs occur. Afterwards, the surface states form a opening arc structure connecting these WPs.

II. STRUCTURE

The optimized lattice constants are $a = 3.074$ Å and $c = 3.513$ Å. These values are in good agreements with previous experimental [48–50] and computational [51–55] results. The structure is shown in Fig. 1(a).

III. PHONON SPECTRA

Figure 1(c) presents the phonon spectrum of MgB_2 along high symmetry momentum paths, which are in nice agreement with previous calculations [51–55] and experimental characterizations [56–58]. At the high-symmetry $K(\frac{1}{3}, \frac{1}{3}, 0)$ and $H(\frac{1}{3}, \frac{1}{3}, \frac{1}{2})$ points, there are three double-degenerate points each. The phonon spectrum along $-H$ to H in Fig. 1(c) evidences the existence of the three double-degeneracy bands, which are PTWNLs in the strictly *straight* lines traversing the whole BZ. In Figs. 1(d) and 1(e), we depicted the phonon dispersions along a PTWNL on the xz plane and around a specified point, $(1/3, 1/3, 0.2)$, in units of the reciprocal lattice vector, of a PTWNL on the xy plane. It can be seen that the dispersion around any point of the PTWNLs exhibits a linear dispersion on the xy plane. It is a hallmark of a WP. In other words, the first, second, and third PTWNLs in Fig. 1(c) are unique. The first, along the $-H$-K-H direction, can be viewed as countless WPs closely aligned in straight lines in its three-dimensional BZ. In the second case, each PTWNL can extend through the whole BZ along this high-symmetry direction in the momentum space. In particular, all of them exactly lie at the BZ boundary along the one-way high-symmetry direction, which are indeed protected by mirror symmetry. In addition, it needs to be emphasized that—although such Dirac nodal-line behaviors stretching the whole BZ along the one-way direction were recently outlined in the electronic structures of rhombohedrally stacked honeycomb lattices [59] and of nanostructured carbon allotropes [60] as well as of the type-II nodal-loop system of K_4P_3 [61]—these symmetry-protected PTWNLs along the one-way direction high-symmetry lines in the phonon spectrum of MgB_2 are still not recognized. Because the symmetries of the phonon momenta obey a C_{3v} point group along the $-H$-K-H direction, the three degenerate lines belong to the E irreducible representation state and the nondegenerate phonon bands belong to the A_1 or A_2 irreducible representation states, respectively [see Fig. 1(c)]. Mechanically, these three different PTWNLs are associated with three distinct phonon modes. The first PTWNL mainly involves the in-plane vibrational mode of Mg atoms, the second one is totally determined by the out-of-plane vibrational mode of two boron atoms moving in opposite or same directions along the c axis while the Mg is stationary, and the third one only involves the in-plane motion in which boron moves along the x or y axes and Mg moves along almost the diagonal direction of the xy axes. Another difference for these three PTWNLs is that the second PTWNL shows an apparent k-dependent dispersion of the frequencies, whereas both the first and third PTWNLs are nearly flat in the frequencies against the k vector along the $-H$-K-H or $-H'$-K'-H' direction, as shown in Fig. 1(c). Furthermore, since the PTWNLs are protected by crystal symmetry, as long as the symmetry is preserved during expansion and shrink of the lattice under a finite temperature, PTWNLs would always present, no matter whether harmonic or anharmonic approximations are considered. We have calculated the expansion coefficient of MgB_2 and used the expanded volume at room temperature to calculate the phonon dispersion. In fact, we have found crystal symmetry protected PTWNLs at room temperature, as shown in the Supplemental Material [47], proving the stability of PTWNLs against the perturbation from a finite temperature.

IV. TOPOLOGICAL PROPERTIES OF PHONONS

To determine the topological nature of these PTWNLs, we have derived the corresponding Berry phase distributions. For a closed loop in the 3D BZ, the Berry phase is defined as

$$\gamma_n = \oint_C \mathbf{A}_n(\mathbf{k}) \cdot d\mathbf{l}, \tag{1}$$

where $\mathbf{A}_n(\mathbf{k}) = i\langle u_n(\mathbf{k})|\nabla_k|u_n(\mathbf{k})\rangle$ is the Berry connection and $u_n(\mathbf{k})$ is the Bloch wave function of nth band. As illustrated in Fig. 1(b), we first selected a closed circle on the xy plane centered at a momentum position of the PTWNL (see the circle marked by the green curves). Note that the radius of the closed circle going around each PTWNL can be selected to be arbitrarily large, as long as it does not also cover another PTWNL. Interestingly, we have found that the Berry phases for all three PTWNLs along the $-H$-K-H direction are π, whereas the other three PTWNLs along the $-H'$-K'-H' direction have an opposite Berry phase of $-\pi$. This means that these PTWNLs are topologically nontrivial, and it also proves that the topological natures of the PTWNLs along the $-H$-K-H direction and $-H'$-K'-H' direction are opposite in their Berry phase due to time reversal symmetry.

In addition, as shown in the phonon spectrum from Γ to A in Fig. 1(c) there are also three twofold-degenerate lines. However, the analysis of their Berry phases and Berry curvatures confirm that these three lines are indeed topologically trivial. Along the Γ to A direction, the symmetries of the phonon momenta obey a C_{6v} point group, the degenerate lines belonging to both E_1 and E_2 states [see Fig. 3(c)]. Due to the degeneracy of both E_1 and E_2 states, which is kept by a C_2 rotation symmetry, the Berry phases of the double-degenerate phonon bands are enforced to be the same. In addition, with the effects of both time reversal and inversion symmetries in the BZ, the Berry phases of the double-degenerate phonon bands along the Γ to A direction have to be opposite. As a result, the Berry phases of the phonon nodal lines along the Γ to A direction are enforced to be zero, being topologically trivial states.

V. PHONONIC DRUMHEAD-LIKE SURFACE STATES

Furthermore, we have identified the surface phonon spectrum of the $(10\bar{1}0)$ surface of MgB_2. As expected, there should be topologically protected phononic nontrivial drumhead-like surface states in the rectangular region confined by the projected lines of the PTWNLs along the K to H direction and along the K' to H' direction. We calculate surface phononic densities of states (PDOSs) by using the iteration Green's function method [62]. After Fourier transforming the force constants, the surface Green's function is built from the dynamical matrix and the surface DOS is taken from the imaginary part of surface Green's function. Figure 2 presents the surface states on the MgB_2 $(10\bar{1}0)$ surface. In Fig. 2(a), we depict the surface PDOSs along high symmetry moment paths on the surface BZ ranging from 12.0 to 16.0 THz to clearly show the phononic surface states associated with the second PTWNL. It can be seen in Fig. 2 that in the $\bar{X}$-$\bar{M}$ direction the bright phononic nontrivial surface states are clearly observable. In Figs. 2(b) and 2(c), we further show the evolutions of drumhead-like surface states with respect to increasing k_z and frequency, respectively. We observe that the surface states are confined well in the rectangular region outlined by the projected lines of two second PTWNLs. In Fig. 2(b), with increasing k_z the downward parabolic-shape nontrivial surface states climb up to a higher frequency and the depth of the parabola becomes smaller and smaller. At $k_z = 0.5$ in Fig. 2(b), the shallow parabolic nontrivial surface states are completely above the surface states at $k_z = 0.0$. This leads to an interesting evolution of the phononic nontrivial surface states as the frequency increases. We have observed three typical types of nontrivial surface states associated with the second PTWNL in Fig. 2(c). When the frequency $13.3 \lesssim f \lesssim 13.9$ THz, the surface states appear to connect two points on the same projected line of the bulk PTWNL. When $13.9 \lesssim f \lesssim 14.8$ THz, the surface states clearly connect two points on the two projected lines of the bulk PTWNLs. When $14.8 \lesssim f \lesssim 15.1$ THz, the surface states form a ring on the 2D surface BZ and do not intersect with any projected lines of the bulk PTWNLs. Indeed, in another two different frequency regions below 12 THz and above 16 THz,

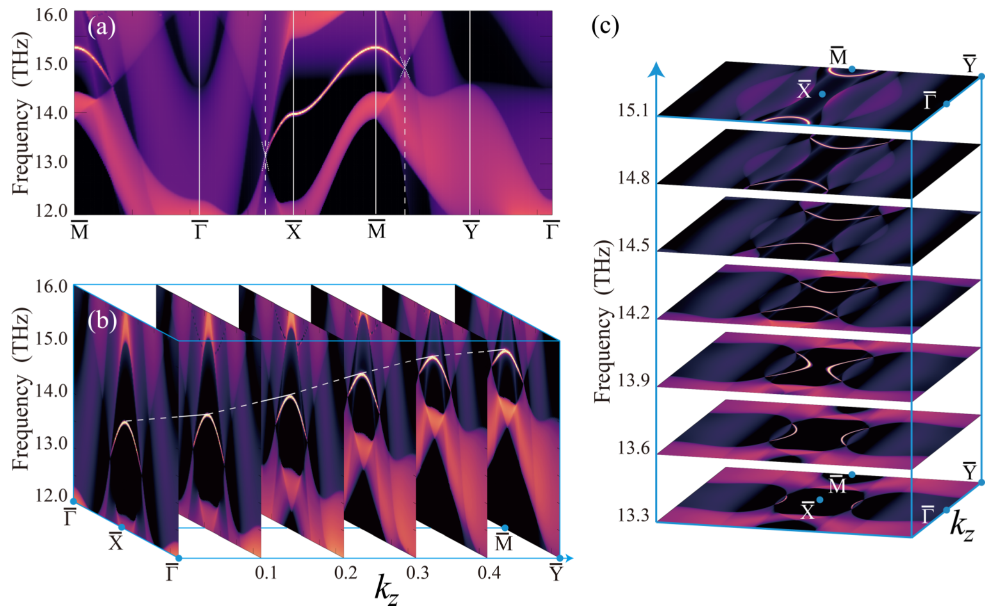

FIG. 2. Phononic states on the $(10\bar{1}0)$ surface of MgB_2. (a) The surface phonon spectrum along high symmetry lines. (b) The evolution of the surface phonon spectra and the topologically protected phononic nontrivial surface states by increasing the k_z value along the $\bar{\Gamma}$-$\bar{X}$-$\bar{\Gamma}$ direction. (c) The frequency-dependent evolution of the phononic surface states of the $(10\bar{1}0)$ BZ as defined in Fig. 1(b) to show the change of the phononic drumhead nontrivial surface states in the rectangular region confined by the projected lines of two PTWNLs with opposite Berry phase.

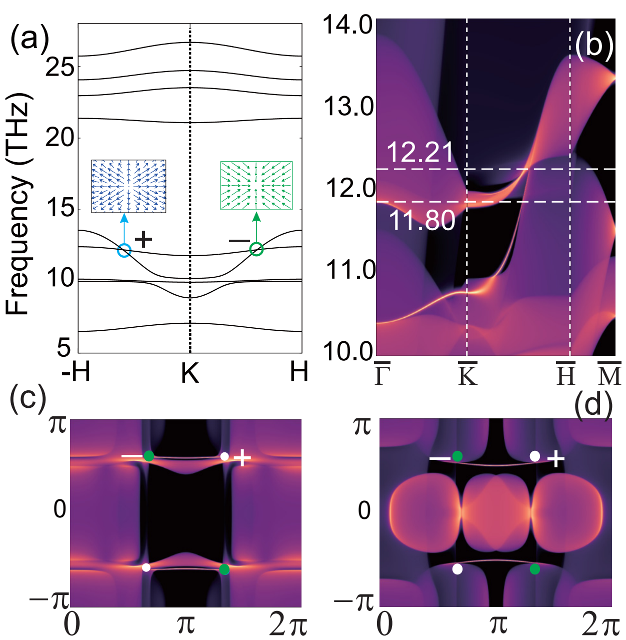

FIG. 3. Phonon dispersion along the $-H$-K-H direction of artificial MgBC and its $(10\bar{1}0)$ surface phonon dispersion. (a) The phonon spectra along the high symmetry $-H$-K-H line. Two WPs are observable with opposite chirality, + and −, as illustrated by Berry curvature distributions in the insets. (b) The surface phonon spectrum along the high-symmetry lines in the $(10\bar{1}0)$ surface BZ to show the nontrivial surface states. Two dashed lines denote the frequencies of 11.80 and 12.21 THz, respectively. Opening arc states connecting a pair WPs with opposite chirality in (c) the surface Fermi-like plot with the frequency of 12.21 THz and (d) the surface Fermi-like plot with the frequency of 11.80 THz.

we can certainly observe the phononic nontrivial surface states which are associated with the first and third PTWNLs along the bulk K-H directions.

VI. PHONONIC WEYL POINTS AND SURFACE ARCS

Interestingly, our calculations also reveal that the double detergency of these PTWNLs can be lifted, possibly resulting in the appearance of WPs, when both the mirror and inversion symmetries are broken. To elucidate this feature, we have substituted one boron atom with a carbon atom in the MgB_2 unit cell, leading to the composition MgBC. With such a treatment, the MgBC structure now belongs to the space group of $P\bar{6}m2$ (No. 187) because the inversion symmetry is broken and, simultaneously, the mirror symmetry of the K-H direction is also broken. As illustrated in Fig. 3(a), the derived phonon dispersion along the H to K direction does not exhibit any PTWNLs due to the lifting up of double degeneracy. In contrast, a pair WPs appear because of the phonon band crossings. We also analyzed their topological nature using the Berry curvature distributions around each WP, obtaining the nonzero topological charges of ± 1 as shown in Fig. 3(a). Additionally, on the $(10\bar{1}0)$ surface we have clearly observed the opening phononic surface arc states connecting to such a pair of WPs with opposite chirality in Figs. 3(b), 3(c), and 3(d).

VII. SUMMARY

From Fig. 2, the PTWNLs in MgB_2 are unique, compared to both Weyl and Dirac nodal-line semimetals. It is well known that a Weyl semimetal results in the appearance of broken Fermi arc states connecting a pair of WPs with opposite chirality [Fig. 4(a)], and a Dirac nodal-line system leads to drumhead-like nontrivial surface states confined in a closed

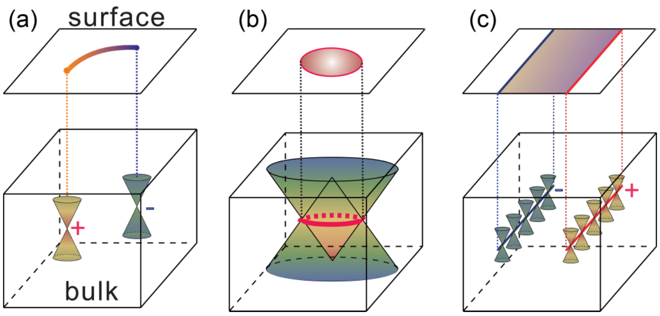

FIG. 4. The diagrammatic comparison of topological (a) Weyl nodes, (b) Dirac nodal lines, and (c) PTWNLs systems. The bulk Weyl nodes, Dirac nodal lines, and PTWNLs are shown in lower panels and their corresponding nontrivial surface states are outlined in the upper panels.

circle-shape region formed by the projected ring of the bulk Dirac nodal lines [Fig. 4(b)]. However, in MgB_2 PTWNLs can be viewed as countless WPs, as in Fig. 4(c), always paired with opposite Berry phase, and they induce drumhead-like rectangular-shape nontrivial surface states, extending the whole surface BZ through the one-way direction. In brief, the PTWNLs-induced nontrivial surface states in Fig. 4(c) can be also viewed as countless broken surface arc states. Available experimental techniques [63–66] to probe these states include neutron scattering, electron energy loss spectroscopy, and x-ray thermal diffuse scattering. Finally, we have found that a series of metallic diborides, such as AlB_2, BeB_2, CaB_2, NaB_2, ScB_2, SrB_2, TaB_2, TiB_2, YB_2, and ZrB_2 (see Supplemental Material [47]), which are isostructural to MgB_2, host similar PTWNLs in their phonon spectra. These metallic diborides, which host PTWNLs, would provide a potential platform to elucidate physical phenomena related to topological phonons, possibly including heat conduction, electrical resistance, and phonon waveguides.

Note added. Recently, we became aware of a publication proposing the electronic topological Dirac nodal lines in MgB_2 through first-principles calculations [67].

ACKNOWLEDGMENTS

This work was supported by the National Science Fund for Distinguished Young Scholars (Grant No. 51725103), by the National Natural Science Foundation of China (Grant No. 51671193), and by the Science Challenging Project No. TZ2016004. All calculations wree performed on the high-performance computational cluster in the Shenyang National University Science and Technology Park.

[1] C. L. Kane and E. J. Mele, Z_2 Topological Order and the Quantum Spin Hall Effect, Phys. Rev. Lett. **95**, 146802 (2005).
[2] M. Z. Hasan and C. L. Kane, *Colloquium*: Topological insulators, Rev. Mod. Phys. **82**, 3045 (2010).
[3] X.-L. Qi and S.-C. Zhang, Topological insulators and superconductors, Rev. Mod. Phys. **83**, 1057 (2011).
[4] S. H. Mousavi, A. B. Khanikaev, and Z. Wang, Topologically protected elastic waves in phononic metamaterials, Nat. Commun. **6**, 8682 (2015).
[5] C. He, X. Ni, H. Ge, X.-C. Sun, Y.-B. Chen, M.-H. Lu, X.-P. Liu, and Y.-F. Chen, Acoustic topological insulator and robust one-way sound transport, Nat. Phys. **12**, 1124 (2016).
[6] Y. Z. Liu, Y. Xu, S.-C. Zhang, and W. H. Duan, Model for topological phononics and phonon diode, Phys. Rev. B **96**, 064106 (2017).
[7] L. Lu, L. Fu, J. D. Joannopoulos, and M. Soljačić, Weyl points and line nodes in gyroid photonic crystals, Nat. Photonics **7**, 294 (2013).
[8] Y. Z. Liu, Y. Xu and W. H. Duan, Berry phase and topological effects of phonons, Natl. Sci. Rev. **5**, 314 (2017).
[9] L. Zhang, and Q. Niu, Chiral Phonons at High-Symmetry Points in Monolayer Hexagonal Lattices, Phys. Rev. Lett. **115**, 115502 (2015).
[10] D. Z. Rocklin, B. G. Chen, M. Falk, V. Vitelli, and T. C. Lubensky, Mechanical Weyl Modes in Topological Maxwell Lattices, Phys. Rev. Lett. **116**, 135503 (2016).
[11] L. Lu, Z. Wang, D. Ye, L. Ran, L. Fu, J. D. Joannopoulos, and M. Soljačić, Experimental observation of Weyl points, Science **349**, 622 (2015).
[12] S. D. Huber, Topological mechanics, Nat. Phys. **12**, 621 (2016).
[13] R. Fleury, A. B. Khanikaev, and A. Alú, Floquet topological insulators for sound, Nat. Commun. **7**, 11744 (2016).
[14] E. Prodan and C. Prodan, Topological Phonon Modes and Their Role in Dynamic Instability of Microtubules, Phys. Rev. Lett. **103**, 248101 (2009).
[15] B. G. Chen, N. Upadhyaya, and V. Vitelli, Nonlinear conduction via solitons in a topological mechanical insulator, Proc. Natl. Acad. Sci. USA **111**, 13004 (2014).
[16] Z. J. Yang, F. Gao, X. H. Shi, X. Lin, Z. Gao, Y. D. Chong, and B. L. Zhang, Topological Acoustics, Phys. Rev. Lett. **114**, 114301 (2015).
[17] P. Wang, L. Lu, and K. Bertoldi, Topological Phononic Crystals with One-Way Elastic Edge Waves, Phys. Rev. Lett. **115**, 104302 (2015).
[18] M. Xiao, W.-J. Chen, W. Y. He, and C. T. Chan, Synthetic gauge flux and Weyl points in acoustic systems, Nat. Phys. **11**, 920 (2015).
[19] L. M. Nasha, D. Klecknera, A. Reada, V. Vitellib, A. M. Turnerc, and W. T. M. Irvinea, Topological mechanics of gyroscopic metamaterials, Proc. Natl. Acad. Sci. USA **112**, 14495 (2015).
[20] R. Süsstrunk and S. D. Huber, Observation of phononic helical edge states in a mechanical topological insulator, Science **349**, 47 (2015).
[21] R. Süsstrunka and S. D. Hubera, Classification of topological phonons in linear mechanical metamaterials, Proc. Natl. Acad. Sci. USA **113**, E4767 (2016).
[22] F. Li, X. Huang, J. Lu, J. Ma, and Z. Liu, Weyl points and Fermi arcs in a chiral phononic crystal, Nat. Phys. **14**, 30 (2018).
[23] T. T. Zhang, Z. D. Song, A. Alexandradinata, H. M. Weng, C. Fang, L. Lu, and Z. Fang, Double-Weyl Phonons in Transition-Metal Monosilicides, Phys. Rev. Lett. **120**, 016401 (2018).
[24] J. X. Li, Q. Xie, S. Ullah, R. H. Li, H. Ma, D. Z. Li, Y. Y. Li, and X.-Q. Chen, Coexistent three-component and two-component

Weyl phonons in TiS, ZrSe, and HfTe, Phys. Rev. B **97**, 054305 (2018).

[25] Q. Xie, J. X. Li, S. Ullah, R. H. Li, L. Wang, D. Z. Li, Y. Y. Li, S. Yunoki, X.-Q. Chen, Phononic Weyl points and one-way topologically protected nontrivial phononic surface arc states in noncentrosymmetric WC-type materials, Phys. Rev. B **99**, 174306 (2019).

[26] C. Fang, H. M. Weng, X. Dai, and Z. Fang, Topological nodal line semimetals, Chin. Phys. B **25**, 117106 (2016).

[27] R. H. Li, J. X. Li, L. Wang, J. X. Liu, H. Ma, H.-F. Song, D. Z. Li, Y. Y. Li, and X.-Q. Chen, Underlying Topological Dirac Nodal Line Mechanism of the Anomalously Large Electron-Phonon Coupling Strength on a Be (0001) Surface, Phys. Rev. Lett. **123**, 136802 (2019).

[28] R. H. Li, H. Ma, X. Y. Cheng, S. L. Wang, D. Z. Li, Z. Y. Zhang, Y. Y. Li, and X.-Q. Chen, Dirac Node Lines in Pure Alkali Earth Metals, Phys. Rev. Lett. **117**, 096401 (2016).

[29] M. Hirayama, R. Okugawa, T. Miyake, and S. Murakami, Topological Dirac nodal lines and surface charges in fcc alkaline earth metals, Nat. Commun. **8**, 14022 (2017).

[30] J. X. Li, H. Ma, Q. Xie, S. B. Feng, S. Ullah, R. H. Li, J. H. Dong, D. Z. Li, Y. Y. Li, and X.-Q. Chen, Topological quantum catalyst: Dirac nodal line states and a potential electrocatalyst of hydrogen evolution in the TiSi family, Sci. China Mater. **61**, 23 (2018).

[31] H. M. Weng, Y. Y. Liang, Q. N. Xu, R. Yu, Z. Fang, X. Dai, and Y. Kawazoe, Topological node-line semimetal in three-dimensional graphene networks, Phys. Rev. B **92**, 045108 (2015).

[32] R. Yu, H. M. Weng, Z. Fang, X. Dai, and X. Hu, Topological Node-Line Semimetal and Dirac Semimetal State in Antiperovskite Cu_3PdN, Phys. Rev. Lett. **115**, 036807 (2015).

[33] Y. Kim, B. J. Wieder, C. L. Kane, and A. M. Rappe, Dirac Line Nodes in Inversion-Symmetric Crystals, Phys. Rev. Lett. **115**, 036806 (2015).

[34] L. S. Xie, L. M. Schoop, E. M. Seibel, Q. D. Gibson, W. W. Xie, and R. J. Cavaa, Line of Dirac Nodes in Hyperhoneycomb Lattices, APL Mater. **3**, 083602 (2015).

[35] K. Mullen, B. Uchoa, and D. T. Glatzhofer, Line of Dirac Nodes in Hyperhoneycomb Lattices, Phys. Rev. Lett. **115**, 026403 (2015).

[36] T. Bzdušek, Q. S. Wu, A. Rüegg, M. Sigrist, and A. A. Soluyanov, Nodal-chain metals, Nature (London) **538**, 75 (2016).

[37] R. Yu, Q. S. Wu, Z. Fang, and H. M. Weng, From Nodal Chain Semimetal to Weyl Semimetal in HfC, Phys. Rev. Lett. **119**, 036401 (2017).

[38] J.-T. Wang, S. M. Nie, H. M. Weng, Y. Kawazoe, and C. F. Chen, Topological Nodal Net Semimetal in a Graphene Network Structrue, Phys. Rev. Lett. **120**, 026402 (2018).

[39] X. M. Zhang, Z.-M. Yu, X.-L. Sheng, H.-Y. Yang, and S. Y. A Yang, Coexistence of four-band nodal rings and triply degenerate nodal points in centrosymmetric metal diborides, Phys. Rev. B **95**, 235116 (2017).

[40] X. Feng, C. G. Yue, Z. D. Song, Q. S. Wu, and B. Wen, Topological Dirac nodal-net Fermions in AlB_2-type TiB_2 and ZrB_2, Phys. Rev. Mater. **2**, 014202 (2018).

[41] Z. H. Liu, R. Lou, P. J. Guo, Q. Wang, S. S. Sun, C. D. Li, S. Thirupathaiah, A. Fedorov, D. Shen, K. Liu, H. C. Lei, and S. C. Wang, Experimental Observation of Dirac Nodal Rings in Centrosymmetric Semimetal TiB_2, Phys. Rev. X **8**, 031044 (2018).

[42] Z. B. Yan, R. Bi, H. T. Shen, L. Lu, S.-C. Zhang, and Z. Wang, Nodal-link semimetals, Phys. Rev. B **96**, 041103(R) (2017).

[43] G. Q. Chang, S.-Y. Xu, X. T. Zhou, S.-M. Huang, B. Singh, B. K. Wang, I. Belopolski, J. X. Yin, S. T. Zhang, and A. Bansil, H. Lin, and M. Z. Hasan, Topological Hopf and Chain Link Semimetal States and Their Application to Co_2MnGa, Phys. Rev. Lett. **119**, 156401 (2017).

[44] R. Bi, Z. Yan, L. Lu, and Z. Wang, Nodal-knot semimetals, Phys. Rev. B **96**, 201305(R) (2017).

[45] X. Feng, Q. S. Wu, Y. Cheng, B. Wen, Q. Wang, Y. Kawazoe, and P. Jena, Monoclinic C_{16}: sp^2-sp^3 hybridized nodal-line semimetal protected by $\mathcal{PT}$-symmetry, Carbon **127**, 527 (2018).

[46] Y. Sun, Y. Zhang, C.-X. Liu, C. Felser, and B. H. Yan, Dirac nodal lines and induced spin Hall effect in metallic rutile oxides, Phys. Rev. B **95**, 235104 (2017).

[47] See Supplemental Material at http://link.aps.org/supplemental/10.1103/PhysRevB.101.024301 for (1) computational methods and details [62,68–75], (2) optimized lattice parameters of a series of metallic diborides, (3) PTWNLs along the $-H$-K-H directions of these metallic diborides, and (4) PTWNL-induced nontrivial phononic surface states for some selected metallic diborides.

[48] J. Nagamatsu, N. Nakagawa, T. Muranaka, Y. Zenitani, and J. Akimisu, Superconductivity at 39 K in magnesium diboride, Nature (London) **410**, 63 (2001).

[49] D. G. Hinks, H. Claus, and J. D. Jorgensen, The complex nature of superconductivity in MgB_2 as revealed by the reduced total isotope effect, Nature (London) **411**, 457 (2001).

[50] M. Jones and R. Marsh, The preparation and sructure of magnesium boride, MgB_2, J. Am. Chem. Soc. **76**, 1434 (1954).

[51] N. I. Medvedeva, A. L. Ivanoskii, J. E. Medvedeva, and A. J. Freeman, Electronic structure of superconducting MgB_2 and related binary and ternary borides, Phys. Rev. B **64**, 020502(R) (2001).

[52] M. J. Mehl, D. A. Papaconstantopoulos, and D. J. Singh, Effects of C, Cu, and Be substitutions in superconducting MgB_2, Phys. Rev. B **64**, 140509(R) (2001).

[53] N. D. Markovskiy, J. A. Muñoz, M. S. Lucas, C. W. Li, O. Delaire, M. B. Stone, D. L. Abernathy, and B. Fultz, Nonharmonic phonons in MgB_2 at elevated temperatures, Phys. Rev. B **83**, 174301(R) (2011).

[54] P. P. Singh, Role of Boron p-Electrons and Holes in Superconducting MgB_2, and Other Diborides: A Fully Relaxed, Full-Potential Electronic Structure Study, Phys. Rev. Lett. **87**, 087004 (2001).

[55] T. Yildirim, O. Gülseren, J. W. Lynn, C. M. Brown, T. J. Udovic, Q. Huang, N. Rogado, K. A. Regan, M. A. Hayward, J. S. Slusky, T. He, M. K. Haas, P. Khalifah, K. Inumaru, and R. J. Cava, Giant Anharmonicity and Nonlinear Electron-Phonon Coupling in MgB_2: A Combined First-Principles Calculation and Neutron Scattering Study, Phys. Rev. Lett. **87**, 037001 (2001).

[56] A. Q. R. Baron, H. Uchiyama, S. Tsutsui, Y. Tanaka, D. Ishikawa, J. P. Sutter, S. Lee, S. Tajima, R. Heid, and K.-P. Bohnen, Phonon spectra in pure and carbon doped MgB_2 by inelastic X-ray scattering, Physica C **456**, 83 (2008).

[57] A. Q. R. Baron, H. Uchiyama, Y. Tanaka, S. Tsutsui, D. Ishikawa, S. Lee, R. Heid, K.-P. Bohnen, S. Tajima, and T. Ishikawa, Kohn Anomaly in MgB_2 by Inelastic X-Ray Scattering, Phys. Rev. Lett. **92**, 197004 (2004).

[58] A. Shukla, M. Calandra, M. D'Astuto, M. Lazzeri, F. Mauri, C. Bellin, M. Krisch, J. Karpinski, S. M. Kazakov, J. Jun, D. Daghero, and K. Parlinski, Phonon Dispersion and Lifetimes in MgB_2, Phys. Rev. Lett. **90**, 095506 (2003).

[59] T. Hyart, R. Ojaärvi, and T. T. Heikkilä, Two topologically distinct Dirac-line semimetal phases and topological phase transitions in rhombohedrally stacked honeycomb lattices, J. Q. Low Temp. Phys. **191**, 35 (2018).

[60] Y. P. Chen, Y. Xie, S. A. Yang, H. Pan, F. Zhang, M. L. Cohen, and S. B. Zhang, Nanostructured carbon allotropes with Weyl-like loops and points, Nano Lett. **15**, 6974 (2015).

[61] S. Li, Z.-M. Yu, Y. Liu, S. Guan, S.-S. Wang, X. M. Zhang, Y. G. Yao, and S. Y. A. Yang, Type-II nodal loops: Theory and material realization, Phys. Rev. B **96**, 081106(R) (2017).

[62] M. P. Lopez Sancho, J. M. Lopez Sancho, J. M. L. Sancho, and J. Rubio, Highly convergent schemes for the calculation of bulk and surface Green functions, J. Phys. F: Metal. Phys. **15**, 851 (1985).

[63] A. Eichler, K.-P. Bohnen, W. Reichardt, and J. Hafner, Phonon dispersion relation in rhodium: *Ab initio* calculations and neutron- scattering investigations, Phys. Rev. B **57**, 324 (1998).

[64] H. Ibach, Surface vibrational studies with electron energy-loss spectroscopy, J. Vac. Sci. Technol. A **5**, 419 (1987).

[65] H. Lourenço-Martins and M. Kociak, Vibrational Surface Electron-Energy-Loss Spectroscopy Probes Confined Surface-Phonon Modes, Phys. Rev. X **7**, 041059 (2017).

[66] R. Xu and T. C. Chiang, Determination of phonon dispersion relations by X-ray thermal diffuse scattering, Z. Kristallogr. **220**, 1009 (2009).

[67] K.-H, Jin, H. Q. Huang, J.-W. Mei, Z. Liu, L.-K. Lim, and F. Liu, Topological Dirac-nodal-line semimetal phase in high-temperature superconductor MgB_2, npj Comput. Mater. **5**, 57 (2019).

[68] G. Kresse and J. Hafner, *Ab initio* molecular dynamics for liquid metals, Phys. Rev. B **47**, 558 (1993).

[69] G. Kresse, and J. Furthmüller, Efficiency of *ab-initio* total energy calculations for metals and semiconductors using a plane-wave basis set, Comput. Mater. Sci. **6**, 15 (1996).

[70] P. Hohenberg and W. Kohn, Inhomogeneous Electron Gas, Phys. Rev. **136**, B864 (1964).

[71] W. Kohn and L. J. Sham, Self-Consistent Equations Including Exchange and Correlation Effects, Phys. Rev. **140**, A1133 (1965).

[72] P. E. Blöchl, Projector augmented-wave method, Phys. Rev. B **50**, 17953 (1994).

[73] J. P. Perdew, K. Burke, and M. Ernzerhof, Generalized Gradient Approximation Made Simple, Phys. Rev. Lett. **77**, 3865 (1996).

[74] A. Togo, F. Oba, and I. Tanaka, First-principles calculations of the ferroelastic transition between rutile-type and $CaCl_2$-type SiO_2 at high pressures, Phys. Rev. B **78**, 134106 (2008).

[75] S. Baroni, S. Gironcoli, A. D. Corso, and P. Giannozzi, Phonons and related crystal properties from density-functional perturbation theory, Rev. Mod. Phys. **73**, 515 (2001).

Correction: The previously published Fig. 1(c) contained errors in the labels for the high-symmetry points and has been replaced.